Ion Transport and Mechanical Properties of Non-Crystallizable Molecular Ionic Composite Electrolytes

Joshua E. Bostwick, ^{1†} Curt J. Zanelotti, ^{2†} Ciprian Iacob, ^{3,4} Andrew G. Korovich, ² Louis A. Madsen, ^{2*} and Ralph H. Colby ^{1*}

¹Department of Materials Science and Engineering, Pennsylvania State University, University Park, Pennsylvania 16802, United States

²Department of Chemistry and Macromolecules Innovation Institute, Virginia Tech, Blacksburg, Virginia 24061, United States

³National Research and Development Institute for Cryogenic and Isotopic Technologies, ICSI, Rm. Valcea 240050, Romania

⁴Institute of Chemical Technology and Polymer Chemistry, Karlsruhe Institute of Technology (KIT), 76131, Karlsruhe, Germany

† Authors contributed equally

Abstract

Polymer electrolytes show promise as alternatives to conventional electrolytes in energy storage and conversion devices but have been limited due to their inverse correlation between ionic conductivity and modulus. In this study, we examine surface morphology, linear viscoelastic, dielectric and diffusive properties of molecular ionic composites (MICs), materials produced through the combination of a rigid and charged double helical polymer, known as poly(2,2')-disulfonyl-4,4'benzidine terepthalamide (PBDT), with ionic liquids (ILs). To probe temperature extremes, we incorporate a non-crystallizable IL to allow measurements from to -90 to 200°C. As we increase PBDT weight percentage (wt%), shear moduli increase and do not decay up to 200°C while maintaining room temperature ionic conductivity within a factor of two of the neat IL. We connect diffusion coefficients of IL ions with ionic conductivity through the Haven ratio across a wide temperature range and analyze trends in ion transport based on a relatively high and

composition-dependent static dielectric constant. This behavior may result from collective rearrangement of IL ions in these networks. We propose that these properties are driven by a two-phase system in MICs corresponding to IL-rich "puddles" and PBDT-IL associated "bundles" where IL ions form alternating sheaths of cations and anions around each PBDT rod. These polymer-based MIC electrolytes show great promise for use in electrochemical devices that require fast ion transport, high modulus, and a broad thermal window.

Keywords:

Polymer electrolyte, ionic liquid, ion gel, modulus, ionic conductivity, diffusion

Introduction

Polymer electrolytes are under investigation for applications in electrochemical energy storage and conversion devices such as lithium ion batteries, fuel cells, solar cells, and sensors, ^{1–5} owing to a combination of high ionic conductivity, mechanical stiffness, and thermal stability. ⁶ Current commercial lithium batteries utilize a combination of organic solvents and a lithium salt to achieve high conductivity but are limited due to dendritic growth and the narrow thermal window and flammability of the organic solvents used. ⁷ To mitigate this, polymer electrolytes in the form of solid single-ion conducting polymers have shown enhancements in some of the properties needed for their use in battery applications but have been stifled due to a reciprocal correlation between stiffness and ionic conductivity. ^{8,9} Stiffer materials that are predicted to prevent dendritic growth typically exhibit less favorable ionic conductivity due to ionic conductivity being coupled with polymer segmental motion. ¹⁰

One technique that has been used to simultaneously achieve high ionic conductivity and mechanical strength is through the introduction of ionic liquids (ILs) into polymeric systems.^{11–14} ILs have gained widespread interest due to their negligible vapor pressure, broad electrochemical window, high ionic conductivity, and thermal stability.^{15–18} Through this combination of ILs and polymers, polymer electrolytes have been produced for energy applications in the form of ion gels.

12,13,19–21 These ion gels have shown high conductivity and a rubber-like modulus due to the interactions between the IL and the polymer matrix.

Alternative to conventional ion gels, another class of materials have been developed, known as molecular ionic composites (MICs) which incorporate the mechanical stiffness of a highly rigid (double helical) sulfonated aramid, poly(2,2'-disulfonyl-4,4'-benzidine terephthalamide)

(PBDT),²² and the favorable ionic conductivity, electrochemical and thermal stability of ILs.¹⁴ Unlike conventional ion gels, which are typically formed from a conventionally physically (hydrophilic-hydrophobic) or chemically crosslinked polymer network, MICs appear to be held together by a collective electrostatic network between the highly charged and highly rigid PBDT rods and the IL ions.²³ While these materials open a new direction in polymer electrolyte fabrication, it is important to understand how the IL and PBDT fractions affect the stiffness and ionic conductivity over a wide temperature range. To explore this, it is important to choose ILs that cannot crystallize because crystallization restricts ion motion in the crystalline domains and greatly decreases overall ionic conductivity.^{24,25} Because of this, non-crystalline ILs need to be incorporated into the PBDT matrix in order to fully study the temperature dependent dynamics of MICs.

In this study, we examine morphology, viscoelastic, dielectric, and individual ion diffusion properties in a series of MICs based on 1-butyl- 3-methylimidazolium tetrafluoroborate (BMIm-BF₄), a non-crystallizable IL, with varying PBDT weight percentage (wt%), and make comparisons with the neat BMIm-BF₄ IL. We studied these responses through a combination of atomic force microscopy (AFM), linear viscoelasticity (LVE), dielectric relaxation spectroscopy (DRS) and NMR diffusometry. Investigating the molecular dynamics of these materials over a wide temperature range enables new insights into the mechanisms of ion transport and mechanical behavior between the IL-PBDT matrix as well as providing new directions for tailoring these electrolyte materials for specific electrochemical applications.

Experimental

Materials: Aqueous solutions of PBDT were produced by combining PBDT and deionized water in vials. BMIm-BF₄ IL was purchased from Iolitec GmbH (Germany) with purity > 99%. **Figure**1 shows structures of both the IL and PBDT as a double helix.

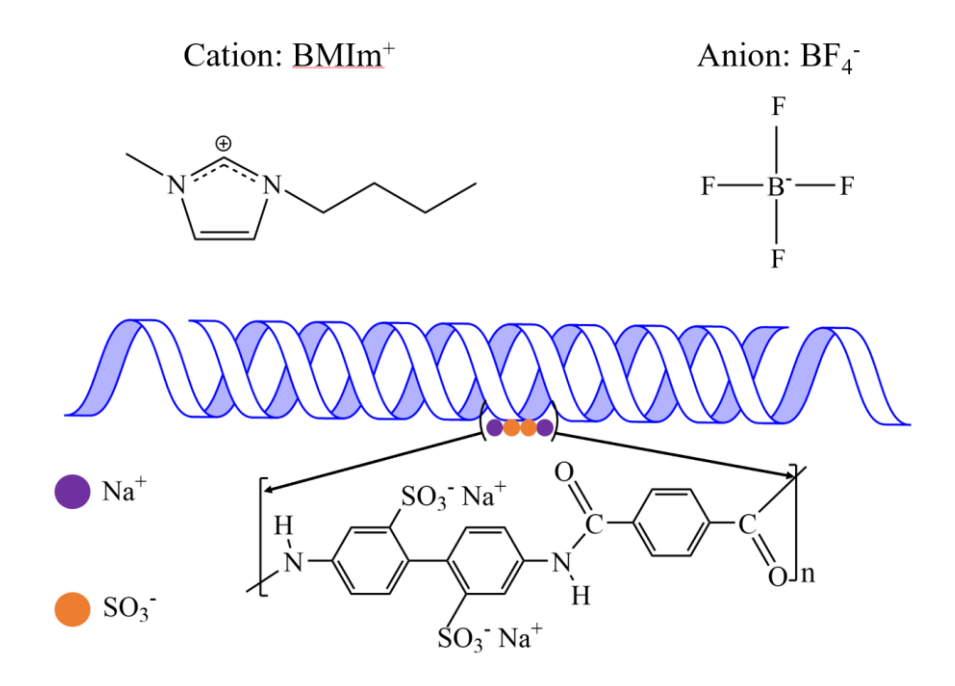


Figure 1: Molecular structures of BMIm⁺ cation, BF₄⁻ anion, and PBDT, with sodium counterions, in a double helical conformation.

Preparation of MICs: Aqueous solutions in the nematic phase 14,22,26 with PBDT ranging from 2-6 wt% were loaded into vials and left for a 3-5 days allowing them to become homogenous. It is important to note that these solutions show a transition to a fully nematic phase at 0.3 wt% PBDT. This PBDT was synthesized from sodium 2,2' benzidinedisulfonate (NaBDSA) and is estimated to have an $M_w \sim 100$ kg/mol based on viscosity measurements. This version of PBDT features longer chains due to the reaction runtime of ~ 24 hours which is much longer than previous PBDT

versions, ^{14,27,28} which were run for ~ 1 hour. Once homogenous, the PBDT solutions were pipetted into 5 mm NMR tubes. IL was then slowly pipetted onto the top of the polymer solution until the IL and PBDT solution volumes were equal. Over time, the IL and water with Na⁺ counterions undergo an ion exchange process in which IL ions diffuse into the PBDT phase and water diffuses into the IL phase shown in **Figure 2**. ¹⁴ Fully formed MIC "ingots" were acquired after 24 h with the solid MIC self-assembling in the region of the original polymer solution. The MICs were then dried in a vacuum oven at 105°C 24 h with resulting PBDT content in the MICs ranging from 4 to 13 wt%. More information involving the formation of MICs can be found from Wang et. al. ¹⁴

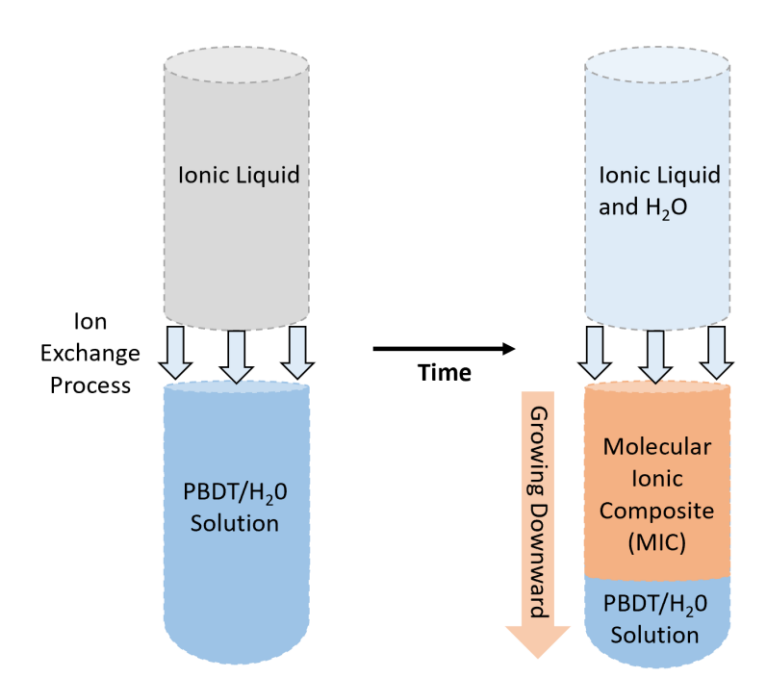


Figure 2: Formation of MIC through an ion exchange process between the IL and the PBDT solution. As time passes, IL ions diffuse into the PBDT phase to self-assemble the MIC phase and cause it to grow downward, while simultaneously and water diffuses into the IL phase.

Atomic Force Microscopy (AFM): AFM images of the three MICs were collected in tapping mode on a Bruker Dimension Icon system using a TESPA-V2 probe tuned to a 0.5 V resonance amplitude. Prior to imaging, each MIC was mounted in a Leica EM UC6 Microtome with a Leica EM FC6 cryo-attachment and sliced with a diamond blade at -110°C to ensure a proper topography on the MIC surface. Each MIC was placed on a stainless-steel substrate and the amplitude setpoint was adjusted for stable topography and good phase contrast ($\sim 0.65 \text{ A}_s/\text{A}_o$ ratio for these samples). Additionally, to ensure the MICs maintained low moisture content under AFM, measurements were done using a humidity chamber at $\sim 20\%$ humidity.

Linear Viscoelasticity (LVE): The viscoelastic response of BMIm-BF₄ IL and MICs of varying PBDT wt% were measured using an Advanced Rheometric Expansion System (ARES)-LS1 rheometer with a transducer measuring 0.2–2000 g cm torque. All ~1 mm thick samples were dried under vacuum for 24 hours at 80° C to remove water and loaded onto aluminum parallel plates with a diameter of 3 mm for the MICs and a combination of 3 mm and 7.9 mm for the neat IL. MICs were annealed in the rheometer for 1 hour at 120° C to insure proper contact with the rheometer plates. The neat IL underwent a shearing process at room temperature to create the precise geometry between the parallel plates. Measurements were taken in steps of 10° C down to the glass transition temperature (T_g), below which measurements were taken in steps of 5° C. At each temperature the shear storage and loss moduli, $G'(\omega)$ and $G''(\omega)$, were recorded in an angular frequency range from $10^{-1} - 10^2$ rad/s in the linear viscoelastic range of strain amplitude. Temperature ramps were also taken for each material at a fixed angular frequency of 1 rad/s and measured in steps of 5° C/min from the glassy modulus up to 200° C.

Dielectric Relaxation Spectroscopy (DRS): Dielectric measurements of MICs and neat IL were carried out through DRS using a Novocontrol GmbH Concept 40 broadband dielectric

spectrometer. All materials were placed under vacuum at 80° C for 24 hours. The MICs of varying PBDT wt% were cut into slices in the direction perpendicular to the elongated axis of the sample and placed in a ring with a diameter of 3 mm and a thickness of 0.575 mm to ensure a proper sample geometry. MICs were then pressed in between a polished 15 mm top brass electrode and a polished 30 mm brass bottom electrode and placed under vacuum at 80° C for 24 hours for the MICs to adhere to the electrodes. BMIm-BF₄ was poured onto a 30 mm brass electrode with an upper electrode diameter of 20 mm and held at a thickness of 0.38 mm using Teflon spacers. Each sample was loaded into the Novocontrol and annealed at 120° C under nitrogen for an additional hour to remove any moisture picked up during sample loading. Isothermal dielectric data were then collected using a sinusoidal voltage with an amplitude of 0.1 V over a frequency range of 10° L in steps of 10° C in cooling from 120 to -150°C followed by steps of 5° C in heating from -150 to 200° C.

NMR Diffusometry: The pulsed-gradient stimulated-echo sequence (PGSTE) was applied for all diffusion measurements from -20 to 150°C. Self-diffusion coefficients of the IL ions were obtained from measuring the nuclei ¹H (cation diffusion) and ¹⁹F (anion diffusion). Before diffusion experiments, all samples were dried and sealed under vacuum to prevent water uptake. Diffusion measurements from -20 to 75°C were performed using a 400 MHz Bruker Avance III WB NMR spectrometer equipped with a microimaging probe coupled to a Diff60 single-axis (z-axis) gradient system and a 5 mm ¹H rf coil. Diffusion measurements from 80 to 150°C were performed using a 600 MHz Bruker Avance III NMR spectrometer equipped DOTY 5 mm, Standard VT, 1H/X high gradient PFG probe. Under pulsed-field-gradient (PFG) NMR diffusometry, the Stejskal-Tanner equation was fit to the measured signal amplitude *I* as a function of gradient strength *g*,

$$I = I_0 e^{-D\gamma^2 g^2 \delta^2 \left(\Delta - \left(\frac{\delta}{3}\right)\right)}$$
 (1)

where I_0 is the signal amplitude at g = 0, γ is the gyromagnetic ratio, δ is the effective gradient pulse duration, Δ is the diffusion time between gradient pulses, and D is the self-diffusion coefficient. The PGSTE sequence used with the Diff60 probe system (-20 to 75° C) used $\pi/2$ pulse lengths of 3.8 and 4.8 μ s for cation (1 H) and anion (19 F), respectively. A repetition time of 0.50 s, a diffusion time of $\Delta = 40$ ms, a gradient pulse length of $\delta = 1.6$ ms, and acquisition times of 40 ms (cation) and 50 ms (anion) were used for cation and anion diffusion measurements. Maximum gradient strengths of 150 - 2100 G/cm, depending on temperature of experiment, were used to achieve 90% signal attenuation in sixteen steps. Sufficient signal-to-noise ratio (SNR) for each data point (> 10) was achieved by acquiring 128 and 64 scans for cation and anion, respectively. The PGSTE sequence used with the DOTY probe system (80 to 150° C) used $\pi/2$ pulse lengths of 41 and 9.2 μ s for cation (1 H) and anion (19 F) respectively. A repetition time of 0.34 s, a diffusion

4.1 and 9.2 μ s for cation (1 H) and anion (19 F), respectively. A repetition time of 0.34 s, a diffusion time of $\Delta = 30$ ms, a gradient pulse length of $\delta = 4.0$ ms, and acquisition times of 100 ms (cation) and 120 ms (anion) were used for diffusion measurements. Maximum gradient strengths of 50 – 180 G/cm, depending on experimental temperature, were used to achieve 90% signal attenuation in sixteen steps. Sufficient signal-to-noise ratio (SNR) for each data point (> 10) was achieved by acquiring 32 and 64 scans for cation and anion, respectively.

Results and Discussion

Morphology of MICs and the Bundle Model

Atomic Force Microscopy (AFM) has been applied in previous studies to elucidate the morphology of IL based composites, as exemplified by Fox et. al.,²⁹ Fam et. al. (in SI),³⁰ and by Ito et. al.³¹ In this case, we used AFM in tapping mode to image the phase contrast for MICs with varying PBDT

wt% as shown in **Figure 3**. These contrast images show dark and bright sections, where brighter areas are the stiffer components in multiphase materials.^{32,33} For MICs, the brighter areas represent regions containing the PBDT phase while darker areas represent regions of nearly neat IL. By increasing the PBDT wt% in MICs, the phase contrast of the overall image gets brighter, suggesting that there is an increased degree of interactions between the PBDT and the IL that drives formation of the MIC.

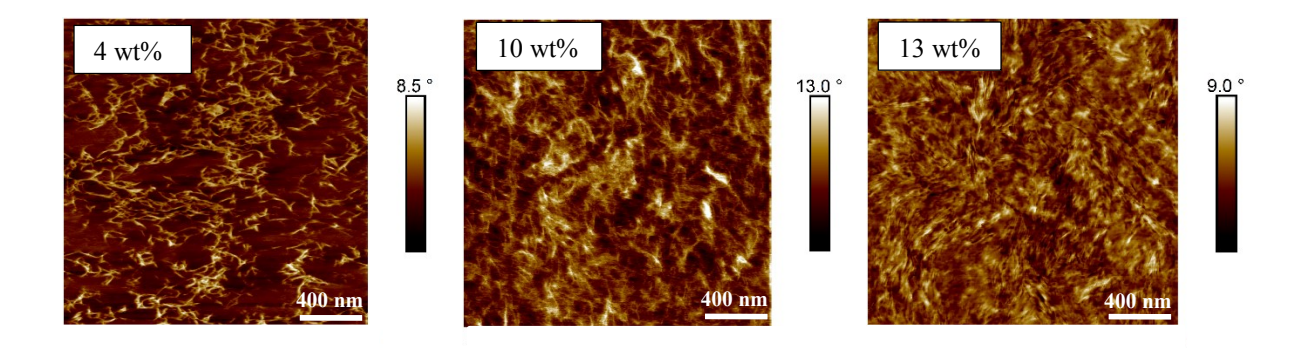


Figure 3: Atomic Force Microscopy (AFM) tapping mode images of the phase contrast in MICs of varying PBDT wt% at room temperature. The images include PBDT wt% and scale bars, with topological and phase contrast angle bars to the right of each image.

Based on these AFM images, on observed compositions where homogenous and mechanically robust MICs form, ^{14,29} and on previous molecular dynamics simulations, ²³ we schematically propose a model for the self-assembled structure of the PBDT rods and IL ions in MICs depicted in **Figure 4**. At low PBDT concentrations, we propose that the internal structure of MICs has two distinct environments, PBDT-rich and PBDT-poor regions. In the PBDT-rich region, we propose that the local environment exists as "bundles" of rigid PBDT rods (blue lines) with each individual rod being surrounded by alternating sheaths of IL cations and anions (purple regions). ²³ These bundles can also form rod-bundle junctions, which may consist of intertwined helical chains (e.g.,

"Y" junctions) along with electrostatic associations that can enhance the mechanical response. In the PBDT-poor region, we propose that the dominant environment is "puddles" of IL (dark red regions). While PBDT rods can still exist within this region, which would attract IL ions, we suspect few PBDT rods are found here. This results in dominant IL motion that is the same as in the neat IL. With increased PBDT concentration, the PBDT-poor regions decrease and are replaced by a larger fraction of PBDT-rich regions. This continues until there are no more PBDT-poor regions and the resulting MIC is dominated by the PBDT-rich environment.

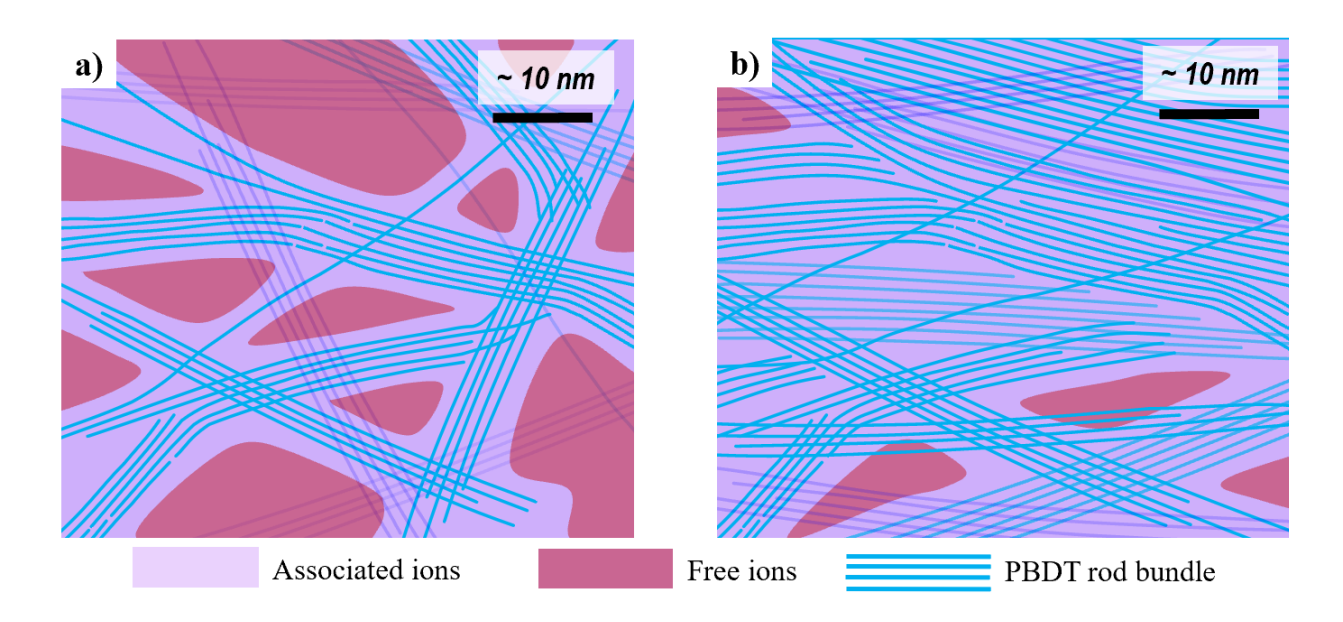


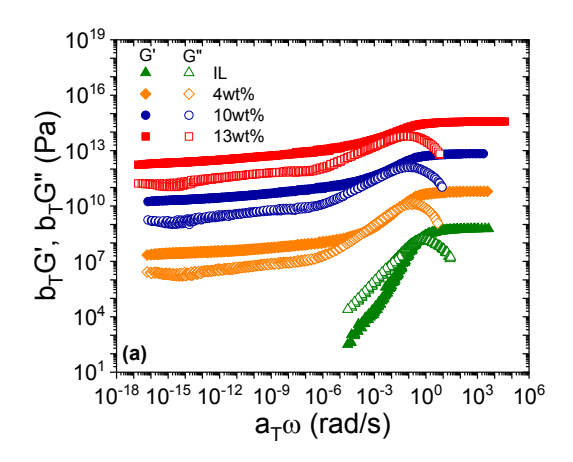
Figure 4: Conceptual illustrations of a nanoscale model of MICs, which includes bundles of PBDT double helix rods (blue lines) (at a rod-rod distance of ~ 2 nm) substantially held together with collective electrostatic (ion-ion) interactions (purple regions). **(a)** MICs at lower PBDT wt% consist of a two-phase system with a continuous PBDT-IL "bundle phase" and pockets or "puddles" (dark red regions) of nearly neat IL. **(b)** MICs at higher PBDT wt% consist primarily of a single PBDT-IL bundle phase, with a small fraction of IL puddles. We discuss our mechanical and ion transport results based on this proposed model.

Linear Viscoelastic Response

To understand how the increase of PBDT wt% affects the mechanical properties of MICs in comparison to neat IL, we examine their linear viscoelasticity (LVE), which allows for the observation of the shear storage and loss moduli (G' and G''). **Figure 5a** shows master curves of the frequency-dependent moduli, $G'(\omega)$ and $G''(\omega)$, obtained for the BMIm-BF₄ IL and MICs with varying wt% of PBDT through time-temperature superposition (tTs). tTs was found to work for all samples with frequency scale shift factors, a_T , shown in **Figure 5b** at a reference temperature $T_r = -85^{\circ}$ C. Each sample exhibited a single α relaxation correlating with the glass transition temperature (T_g) of the system denoted by the maximum peak in $G''(\omega)$. To determine T_g of the neat IL and MICs through LVE, we fit the frequency scale shift factors from the tTs master curves using the Williams-Landau-Ferry (WLF) equation.³⁴

$$\log a_T = -\frac{C_1(T - T_r)}{C_2 + T - T_r} \tag{2}$$

Here, C_1 and C_2 are fit parameters, T is the temperature and T_r is the reference temperature. Using C_1 and C_2 , $G''(\omega)$ was shifted until we observed the maximum peak at a frequency of 10^{-2} rad/s indicating T_g . Table 1 shows the fitting parameters for the IL and MICs as well as the T_g determined through LVE, and our measurements are in agreement with previous work done calculating the LVE T_g of BMIm-BF4. Increasing the PBDT wt% in MICs only slightly increases T_g by 2 K, suggesting that the IL ions dictate the viscoelastic T_g even at our highest PBDT wt% MIC. We suspect that the LVE T_g originates from rearrangement of IL ions 35,37,38 and this idea of IL motion at T_g is consistent with the molecular structures shown in **Figure 4** where IL ions within the puddles are able to move freely with minimal restriction from the PBDT bundles.



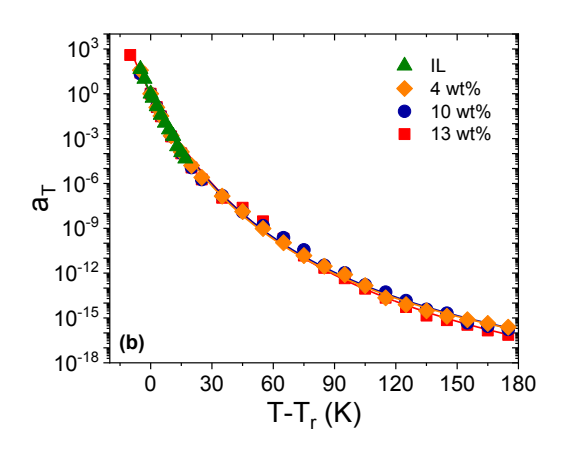


Figure 5: (a) Time–temperature superposition master curves of the frequency-dependent shear storage and loss moduli, $G'(\omega)$ and $G''(\omega)$, for BMIm-BF₄ IL and MICs of varying PBDT wt% at a reference temperature $T_r = -85^{\circ}$ C. For easy viewing, we vertically shifted these curves by a factor b_T where b_T(BMIm-BF₄) = 1, b_T(4 wt% MIC) = 100, b_T(10 wt% MIC) = 10000, and b_T(13 wt% MIC) = 500000. (b) Viscoelastic horizontal shift factors, a_T versus temperature for BMIm-BF₄ IL and MICs of varying PBDT wt% for the master curves in part (a) at a reference temperature $T_r = -85^{\circ}$ C. The solid lines represent the fits from the WLF equation (Eq. 2) with the fitting parameters listed in **Table 1**. Increasing PBDT content only slightly increases the glass transition temperature (T_g) while showing a weak frequency-dependence of the modulus, indicating that MICs are viscoelastic solids.

Table 1: Fitting parameters of the WLF temperature dependence (Eq. 2) with $T_r = -85^{\circ}$ C and								
LVE glass transition temperature (T_g)								
Sample	C_1	$C_2(K)$	$T_0 = T_{r} - C_2 (K)$	$LVE^{a} T_{g}(K)$				
BMIm-BF ₄	27.8	92.4	95.6	181				
4 wt% MIC	23.1	82.3	105.7	183				
10 wt% MIC	23.3	85.5	102.5	183				
13 wt% MIC	24.8	93.9	94.1	183				

 aT_g determined through LVE measurements defined where $\omega_o(T_g) = 10^{-2}$ rad/s at which G" has a maximum in the glassy regime indicating segmental relaxation.

As PBDT content increases in MICs, the shear storage modulus increases from 0.2 to 4 MPa at room temperature and isothermal frequency sweeps shows minimal variation of the modulus

above room temperature in $G'(\omega)$ and $G''(\omega)$, indicating MICs are viscoelastic solids.³⁹ To further illustrate this effect of the IL-rich puddles on the viscoelastic response of MICs, we examine the ratio between the glassy modulus (G_g) and the plateau modulus (G_e) where $G_e = G'(10^{-15} \text{ rad/s})$ as shown in **Figure 6**. As the PBDT content increases, G_g/G_e decreases suggesting that the change in modulus directly relates to the volume fraction of the IL-rich puddles. Since the IL ions are the dominant source of viscoelastic relaxation in MICs, they can relax in the IL-rich puddles, causing MICs to possess a low T_g comparable to the neat IL. However, by increasing the PBDT content in MICs, the volume fraction of the IL puddles decreases, forcing the majority of the IL ions to relax within the PBDT bundles and increasing G_e due to the interactions between PBDT and IL. We will discuss this concept further below.

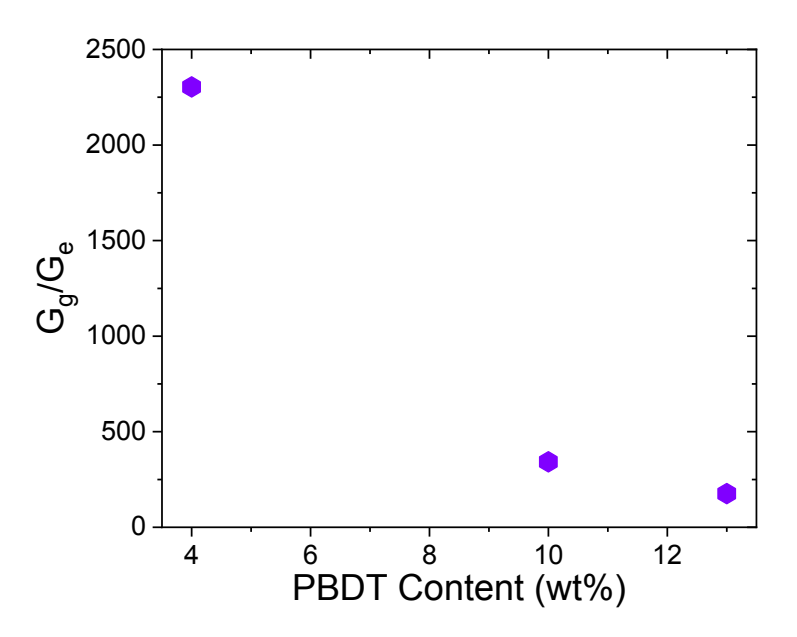


Figure 6: G_g/G_e as a function of PBDT wt% in MICs. G_g/G_e decreases as PBDT content increases suggesting that the modulus change is directly associated with to the decreased volume fraction of IL-rich puddles.

In addition to the frequency-dependence of the modulus, we also analyzed the modulus as a function of temperature at $\omega=1$ rad/s, as illustrated in **Figure 7**. Here, the absence of terminal liquid response is further shown as G' and G'' leave the glassy state, reach a plateau and exhibit a weak temperature dependence at elevated temperatures. MICs never terminally relax at higher temperatures, similar to the LVE of crosslinked rubbers⁴⁰ but their modulus also does not weakly increase with temperature as in crosslinked rubbers,³⁹ further emphasizing the novel behaviors in these ionic network composites. Although the moduli of MICs are of MPa order, they do not exhibit the entropic origins of crosslinked polymers and many soft materials. We hypothesize that this may be due to collective weak ionic interactions between the PBDT rigid rods and IL ions. Negatively charged PBDT rods are surrounded by sheaths of BMIm⁺ cations and BF₄⁻ anions, forming an electrostatic network that spans throughout the MIC and allowing the MIC to be thermally and mechanically stable at elevated temperatures.²³ Additionally, as temperature increases, we observed a slight increase in G'' for all MIC samples which agree with previous dynamic mechanical thermal analysis done on similar MIC samples.²⁹

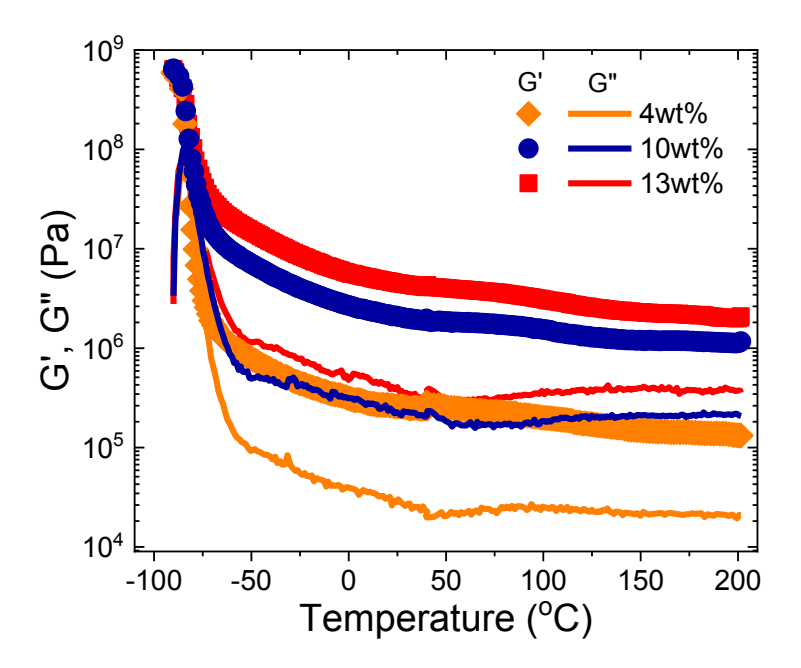


Figure 7: Temperature-dependence of G' and G" for MICs of varying PBDT wt% at an angular frequency of 1 rad/s. From -50°C to 200°C, the storage modulus exhibits a gradual decrease as temperature is raised, suggesting that the MIC modulus does not have the entropic origins that many soft materials have.

It is important to note that we observed modulus values that are much lower than previous studies on the modulus of MICs. ^{14,29} Based on our preliminary findings, we expect that this is may be due to different aspects of MIC composition and formation. MICs produced in this study used a different IL than previously studied and we hypothesize that the specific and collective molecular interactions present in MICs can alter the modulus. Additionally, while it is typical for shear modulus to be lower than Young's modulus, these materials exhibit differences in moduli by factors of ten or more, suggesting that the modulus may be anisotropic. This may originate from the anisotropic electrostatic network that is involved in the energetics of mechanical deformation. ⁴¹ Finally, we also have preliminary observations suggesting that the molecular weight of the PBDT strongly influences both the formation process and the final modulus. We

speculate that the higher molecular weight PBDT used in this study may kinetically arrest the composite during formation and thus form disjointed structures. When a MIC was made with this version of PBDT and a different IL (1-ethyl- 3-methylimidazolium trifluromethanesulfonate,) the tensile modulus was lower by a factor of ~ 100 compared to what was previously found (33 MPa vs. 3 GPa). While molecular weight can drastically affect the modulus, we observed no change in the measured conductivity or diffusion, suggesting that PBDT chain lengths do not substantially affect fast ion transport. Future studies will probe in further detail how mechanical and transport properties in MICs depend on PBDT and IL molecular details, thus enabling fine material property tuning for electrochemical device applications.

Ionic Conductivity

In order to investigate the influence of PBDT wt% on MICs, we analyze the temperaturedependence of ionic conductivity (σ_0) in the regime where ε " $\sim \omega^{-1}$ and $\sigma_0 = \omega \varepsilon_0 \varepsilon$ ", and we compared with the neat IL.^{42–44} Shown in **Figure 8**, we fit σ_0 data using the Vogel-Fulcher-Tammann (VFT) equation, ^{45,46}

$$\sigma_o(T) = \sigma_\infty \exp\left(-\frac{BT_0}{T - T_0}\right) \tag{3}$$

where σ_{∞} is the infinite temperature conductivity limit, B is a strength parameter proportional to fragility, and T_0 is the Vogel temperature listed in **Table 2**. By fitting VFT to σ_0 , we show that the T_0 determined from DRS is at least 50 K higher than that from the T_0 determined by LVE methods for all samples. We believe this is due to the difference in mechanisms dictating the mechanical and dielectric responses. While DRS is analyzing T_0 in both the IL-rich puddle phase

and PBDT bundle phase, T_0 from LVE is mostly influenced by the relaxation of ions in the IL-rich puddles near T_g .

While all samples show similar trends in conductivity, increasing PBDT wt% only slightly decreases σ_0 in MICs. This decrease is never more than a factor of two relative to that of the neat IL at room temperature, from 4.4 mS/cm to 2.2 mS/cm at the highest PBDT content MIC (13 wt%). At 200°C, σ_0 of MICs reaches 60-70 mS/cm regardless of PBDT wt%, and the MICs still exhibit a conductivity $\geq 10^{-5}$ S/cm above -30°C. When compared to a wide array of other solid polymer-based electrolytes, MICs show a comparable or higher ionic conductivity,²⁹ and over a much wider temperature window than previously reported in literature. We expect these comparably high σ_0 values partially relates to two distinct ionic environments in MICs, which correlate with the IL-rich puddles and the bundles of PBDT rods shown above in **Figure 4**. At low PBDT concentrations, these PBDT-poor puddles of free IL exhibit the transport rates of neat IL due to the absence of the PBDT rods. As PBDT concentration increases, these puddles decrease in size and the majority of ions travel within the bundles of PBDT rods where the sheaths of IL have ion motions only somewhat slower compared to the neat IL. Additionally, while increasing the PBDT content increases the number of associations between IL ions and the sulfonate group fixed on the polymer backbone, these associated ions diffuse on relatively fast time scales, maintaining high σ_0 as the PBDT wt% increases in the MIC.²³ We further discuss the effect on PBDT content of ion diffusion below.

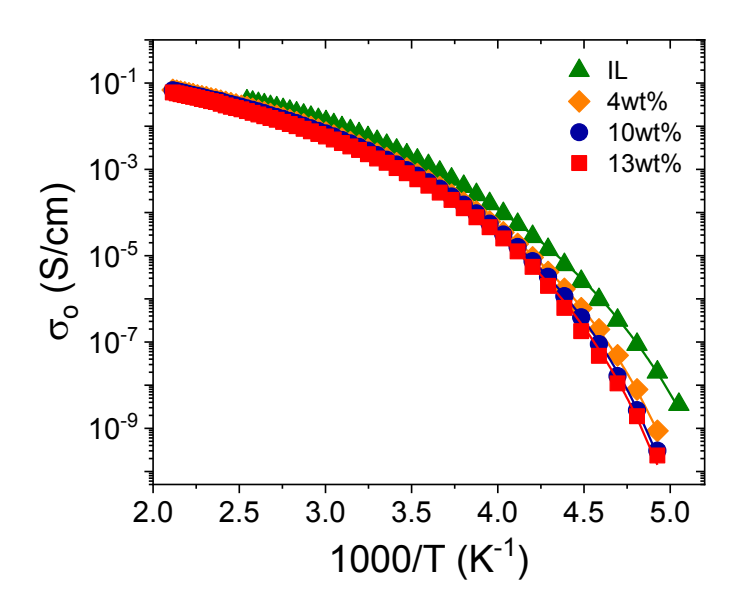


Figure 8: Temperature dependence of ionic conductivity (σ_0) for neat BMIm-BF₄ IL and for MICs of varying PBDT wt%. The solid lines represent the fits using the VFT equation (Eq. 3) with parameters listed in **Table 2**. MICs show fast ion transport over a wide temperature range, and this transport is not much slower than that of the neat IL.

Table 2: Fitting parameters from the VFT temperature dependence (Eq. 3) of ionic								
conductivity and static dielectric constant (ε_s) at -20°C								
Sample	$\log \sigma_{\infty}$ (S/cm)	B $T_0(K)$		$\mathcal{E}_{ ext{S}}$				
BMIm-BF ₄	0.52	7.1	148	14.3				
4 wt% MIC	0.19	6	158	12.8				
10 wt% MIC	0.14	5.7	162	16.1				
13 wt% MIC	0.12	5.8	162	23.5				

Static Dielectric Constant

We analyze the static dielectric constant (ε_s) to illustrate how MICs become more polarizable as PBDT wt% increases. **Figure 9** shows the frequency-dependence of the real part of the dielectric

permittivity (ε ') at -20°C for BMIm-BF₄ IL and for MICs of varying PBDT wt%. In order to account for all relaxations that occur between the IL and PBDT prior to electrode polarization (EP), we probe ε_s , defined as the low frequency value of ε ' prior to EP. ε ' represents the summation of all observed relaxations in MICs and we plot this as a solid line in the low frequency limit of ε '. $^{49-52}$ The value of ε_s for the IL is \sim 14 which is similar to previous studies on the dielectric constant of BMIm-BF₄. 53,54 As the PBDT wt% increases, ε_s in MICs becomes greater than that of the IL reaching a value of 23.5. We expect that the increase in ε_s is due to the presence of the PBDT rods. We propose that increasing the PBDT wt% leads to more strongly correlated ion rearrangements in the IL ions between the PBDT rods, facilitating an increase in polarizability. This enhanced polarizability likely explains the high conductivity of the PBDT-IL phase in the MICs. Enhancing the static dielectric constant should lead to an increase in conductive ions that can be accounted for in DRS. 55

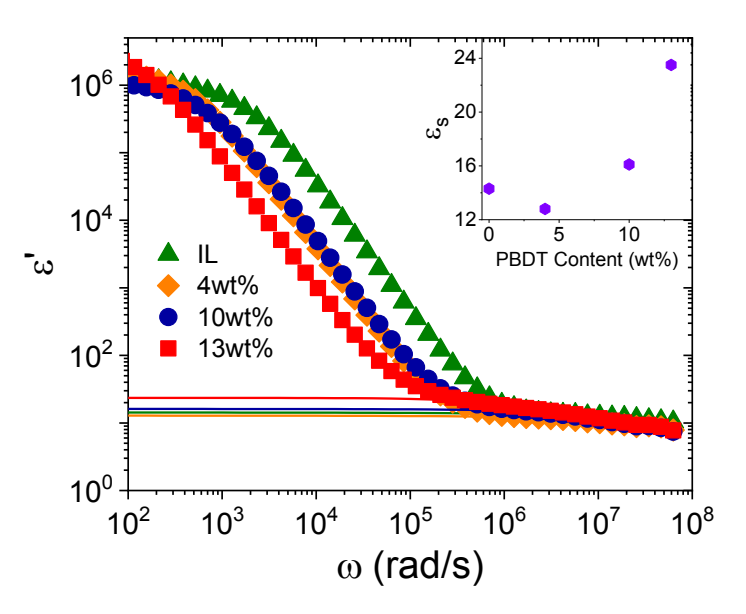


Figure 9: Real permittivity (ε ') at -20°C for BMIm-BF₄ IL and for MICs of varying PBDT wt%. The solid lines represent the static dielectric constant (ε _s) determined by the summation of the dielectric constants of all observed relaxations prior to electrode polarization (EP), and we list

these values in in **Table 2**. **Inset:** ε_s as a function of PBDT wt% in MICs. The increase in ε_s with PBDT content suggests that the PBDT-rich bundle phase is highly polarizable.

Diffusion of Ionic Liquid in MICs

In order to further explore MIC ion transport behaviors, we employ pulsed-field-gradient (PFG) NMR diffusometry to separately quantify self-diffusion coefficients for the BMIm⁺ cation and BF₄⁻ anion in each MIC and in neat IL. **Figure 10a** compare the cation and anion diffusion coefficients between the neat IL and the MIC with 13 wt% PBDT. In both neat IL and the MIC, the BMIm⁺ cation shows slightly faster diffusion than the BF₄⁻ anion at $T < 80^{\circ}$ C. At $T > 80^{\circ}$ C, BF₄⁻ anion diffusion becomes slightly faster. Additionally, the 13 wt% MIC shows cation and anion coefficients that are comparable to the neat IL This is due to the ions' ability to rapidly diffuse among the PBDT bundles. ^{14,23,56,57} We might expect that the BMIm⁺ cations will diffuse much slower in an anionic matrix due to their associations with the fixed sulfonated groups off of the polymer backbone. However, because the interactions between the IL and the PBDT rods are weak, these associated ions will only have a very short lifetime (a few ns)²³ on the fixed sulfonate groups meaning that these ions are diffusing and exchanging with dissociated ions over this quick timescale.

To understand the temperature-dependent diffusion behavior and its comparison with ionic conductivity (σ_0), we have fit the cation and anion diffusion coefficients using the VFT equation,

$$D_o(T) = D_{\infty} \exp\left(-\frac{BT_0}{T - T_0}\right) \tag{4}$$

where D_{∞} is the infinite temperature diffusion limit, B is a strength parameter and T_0 is the Vogel temperature listed in **Table 3**. For a proper comparison of σ_0 and self-diffusion, we fix T_0 to the

same Vogel temperature found from the VFT fit of the σ_0 as that data set covers a broader temperature range. **Figures 10b** and **10c** show diffusivity fitted to the VFT equation. Increasing the PBDT wt% in the MICs leads to a decrease in the diffusion coefficient, paralleling the trends shown in σ_0 . Additionally, fixing T_0 in the VFT equation to the T_0 from σ_0 for each of the samples lead to good agreement in the diffusion data suggesting that σ_0 and diffusion processes correlate well with one another.

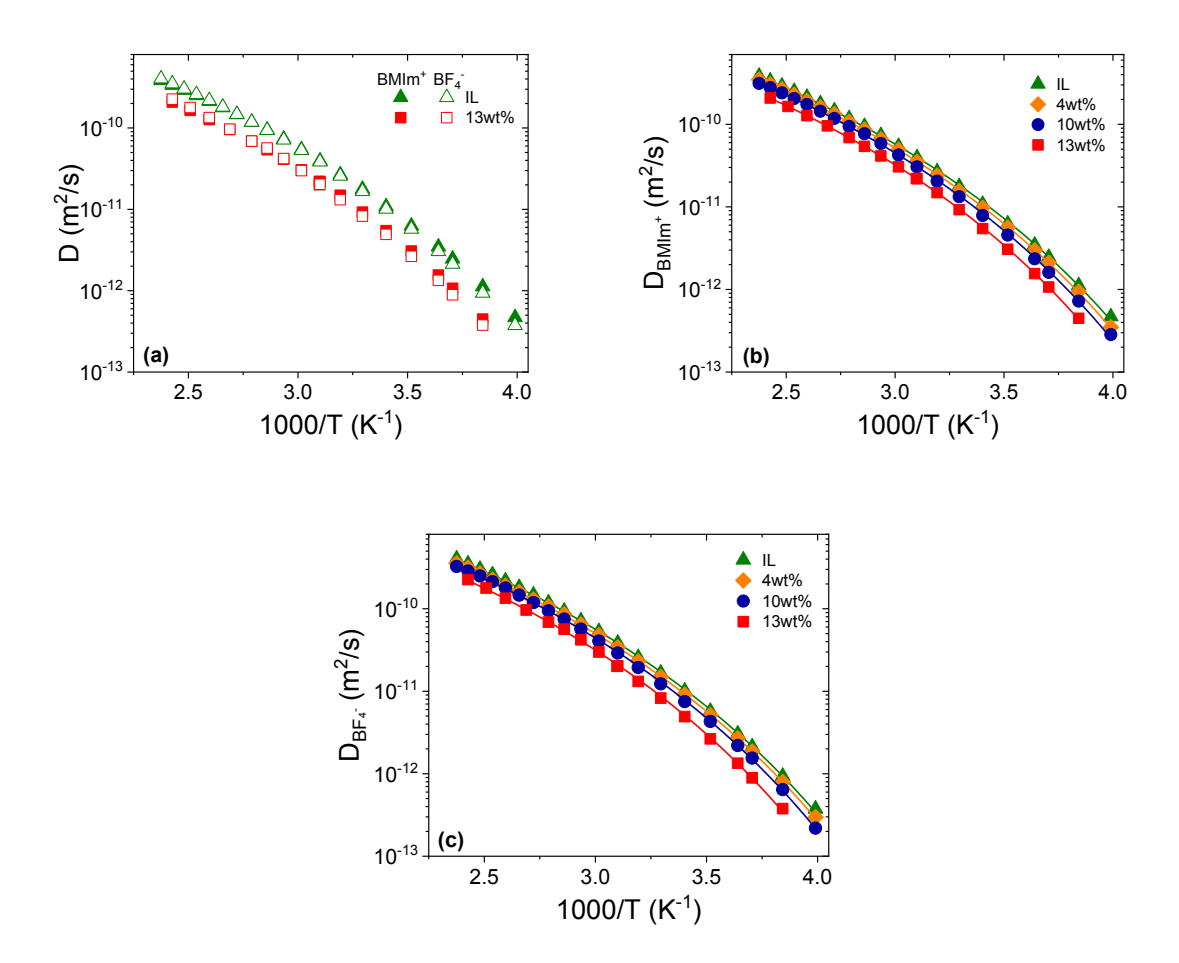


Figure 10: (a) Comparison of the cation and anion diffusion coefficients for the neat IL and for MIC with 13 wt% PBDT. Temperature-dependence of the **(b)** cation diffusion, $D_{\rm BMIm}^+$, **(c)** anion diffusion, $D_{\rm BF4}^-$, for neat IL and for all MIC samples. Solid lines are fits to the VFT equation (Eq. 4) with parameters listed in **Table 3**. Ion diffusion coefficients only mildly reduce inside MICs, and the temperature dependencies of IL and MICs match almost exactly. Above 80°C,

anions are slightly faster than cations while cations are slightly faster below 80°C, indicating a mild change in ion association behavior with temperature.

Table 3: Fitting parameters from the VFT temperature dependence (Eq. 4) for the cation and anion diffusion coefficients									
	D_{BMIm}^+			$D_{ m BF_4}^-$					
Sample	$\log D_{\infty} (\mathrm{m^2/s})$	В	$T_0(K)$	$\log D_{\infty} (\mathrm{m^2/s})$	В	$T_0\left(\mathbf{K}\right)$			
BMIm-BF ₄	-7.6	7.5	148	-7.5	7.8	148			
4 wt% MIC	-7.8	6.3	158	-7.8	6.5	158			
10 wt% MIC	-7.9	5.9	162	-7.9	6.1	162			
13 wt% MIC	-8	6.2	162	-7.9	6.4	162			

Nernst-Einstein Equation and the Haven Ratio

We can further assess the effects of ionic interactions in MICs by comparing diffusion coefficients with ionic conductivities. In the limit of freely moving ions, with no interactions among them, ionic conductivity should be related to the diffusion coefficients from NMR through the Nernst-Einstein equation, 58 which in this case is

$$\sigma_o = \frac{p_{IL}e^2}{H_PkT} \left(D_{BMIm^+} + D_{BF_4^-} \right)$$
 (5)

where σ_0 is the ionic conductivity, $D_{\rm BMIm}^+$ and $D_{\rm BF4}^-$ are the temperature-dependent diffusion coefficients for the cation and anion respectively from NMR, $p_{\rm IL}$ is the number density of each IL

ion, e is the elementary charge, H_R is the Haven ratio and kT is thermal energy. This equation neglects the number density and the diffusion coefficient of the Na⁺ counterions from the PBDT because the number density of IL ions is much higher and the diffusion coefficients of IL ions are potentially greater than that of the Na⁺ counterions. H_R represents the ratio between the conductivity determined through NMR over the ionic conductivity determined through DRS. 59-61 A Haven ratio of unity indicates that the diffusion of all ions present is properly accounted for in ionic conductivity, meaning that ions move independently as in a dilute solution. Figure 11 shows the H_R as a function of temperature, and for all samples $1 \le H_R \le 2$, suggesting that the Nernst-Einstein equation works reasonably well for this class of materials. 62 The trends in $H_{\rm R}$ are similar to previous results by Watanabe et al. on ILs where H_R is nearly independent of temperature. ⁶³ The 4 wt% and 10 wt% MIC samples have similar H_R values to the neat IL, possibly representative of ion pairs that do not contribute to ionic conductivity, 58,64 or other ionic aggregates that contribute less strongly than separated ions. 56,57 However, the 13 wt% sample has an H_R value close to 1. This may be due to the relatively high static dielectric constant causing an increase in conductive ions that are present through DRS. Additionally, this suggests that at higher PBDT wt%, ionic interactions between the PBDT and IL within their closely associated bundles play a role in a lowering H_R . By increasing the PBDT wt%, free IL puddles in the MIC shrink, shown earlier in Figure 4b, leading to formation of a near single PBDT-IL bundle-dominated phase.

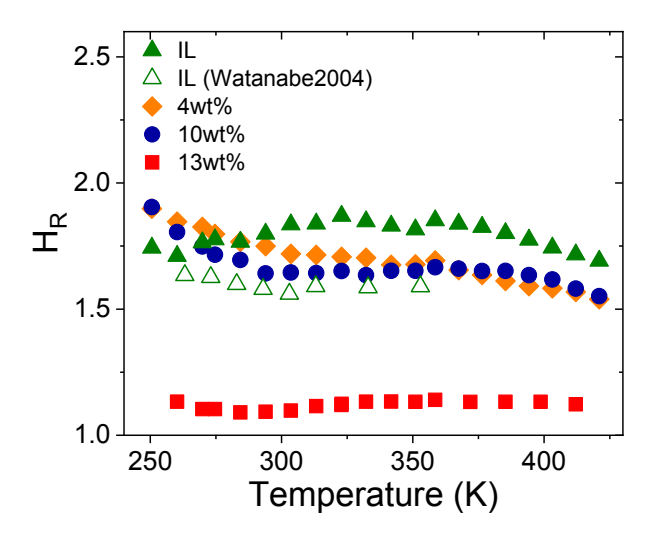


Figure 11: Temperature-dependence of the Haven ratio, determined through Eq. 5, for BMIm-BF₄ IL and MICs of varying PBDT wt%. Open green triangles represent the Haven ratio data of BMIm-BF₄ from Watanabe et al.⁶³ Increasing PBDT content causes more dissociated ions to contribute to the ionic conductivity due to an increase in the static dielectric constant as well as the formation of a near single PBDT-IL bundle dominated phase.

Conclusions

In this study, we examine molecular ionic composites (MICs) based on a combination of poly(2,2'-disulfonyl-4,4'-benzidine terephthalamide (PBDT) and the non-crystallizable ionic liquid (IL) 1-butyl- 3-methylimidazolium tetrafluoroborate (BMIm-BF4) as a function of PBDT wt%. We analyze the surface morphology as well as the macroscopic mechanical and ionic dynamics through shear rheology, dielectric and ion diffusion measurements. As PBDT wt% increases, shear modulus increases into the MPa range while ionic conductivity shows a minimal decrease, by approximately a factor of two, when compared to the neat IL at room temperature. We discuss this combination of simultaneous high modulus and conductivity in terms of two phases in MICs, an IL-rich "puddle" phase and a PBDT-IL "bundle" phase which allow for the IL and PBDT to contribute to the mechanical and dielectric dynamics simultaneously. We show that this ionic

conductivity is higher than other solid polymer-based electrolytes, ²⁹ and spans a wide temperature

window. Linear viscoelastic measurements show that the shear modulus has only very weak

frequency and temperature dependences above room temperature, with a minimal increase in glass

transition temperature (T_g) by 2 K due to the segmental motion of the IL.

NMR diffusometry illustrates that the diffusion of cations and anions in the neat IL and in the

highest wt% MIC are comparable due to the ions' ability to diffuse quickly among PBDT chains.

We correlate ionic diffusion with ionic conductivity through the Nernst-Einstein equation and the

Haven ratio, which shows values between one (high PBDT wt% MICs) and two (low PBDT wt%

MICs or neat IL). This dependence suggests that more ions contribute to conduction when a nearly

single phase of PBDT-IL bundles exist throughout the MIC and that correlated ion rearrangements

cause a relatively high static dielectric constant. These materials exhibit distinctly new phenomena

and show promise as a new and tunable platform for high modulus electrolytes with fast ion

transport.

Associated Content

Supporting Information

Isochronal conductivity showing reproducible ionic conductivity values, restricted (variable

diffusion time) diffusion studies, variation of Vogel temperature from diffusion data.

Author Information

Corresponding Authors

*Email: rhc@plmsc.psu.edu (R.H.C)

*Email: lmadsen@vt.edu (L.A.M)

ORCID

26

Joshua E. Bostwick: 0000-0002-0640-5223

Curt J. Zanelotti: 0000-0003-2622-7345

Ciprian Iacob: 0000-0001-7982-0586

Andrew G. Korovich: 0000-0003-3736-1523

Louis A. Madsen: 0000-0003-4588-5183

Ralph H. Colby: 0000-0002-5492-6189

Notes

The authors declare no competing financial interest.

Acknowledgements

The authors would like to thank Professor James Runt for helpful discussions, Missy Hazen for cryo-cutting the MICs prior to AFM characterization, Timothy B. Tighe and Teague A. Williams for AFM characterization, Maruti Hedge and Theo J. Dingemans for providing the PBDT polymer, and Ryan J. Fox for providing elastic modulus on a MIC sample. This work was supported by the National Science Foundation under the awards DMR 1807934, 1507764, and 1810194 and we thank them for funding this project.

References

- (1) Arya, A.; Sharma, A. L. Polymer Electrolytes for Lithium Ion Batteries: A Critical Study. *Ionics* **2017**, *23* (3), 497–540.
- (2) Wang, Y.; Chen, K. S.; Mishler, J.; Cho, S. C.; Adroher, X. C. A Review of Polymer Electrolyte Membrane Fuel Cells: Technology, Applications, and Needs on Fundamental Research. *Appl. Energy* **2011**, *88* (4), 981–1007.
- (3) Arof, A. K.; Noor, I. M.; Buraidah, M. H.; Bandara, T. M. W. J.; Careem, M. A.; Albinsson, I.; Mellander, B. E. Polyacrylonitrile Gel Polymer Electrolyte Based Dye Sensitized Solar Cells for a Prototype Solar Panel. *Electrochim. Acta* **2017**, *251*, 223–234.
- (4) Opekar, F.; Štulík, K. Electrochemical Sensors with Solid Polymer Electrolytes. *Anal. Chim. Acta* **1999**, *385*, 151–162.
- (5) Young, W. S.; Kuan, W. F.; Epps, T. H. Block Copolymer Electrolytes for Rechargeable Lithium Batteries. *J. Polym. Sci. Part B Polym. Phys.* **2014**, *52*, 1–16.
- (6) Lodge, T. P. Materials Science: A Unique Platform for Materials Design. *Science* **2008**, *321* (5885), 50–51.
- (7) Takehara, Z. Future Prospects of the Lithium Metal Anode. *J. Power Sources* **1997**, *68*, 82–86.
- (8) Snyder, J. F.; Carter, R. H.; Wetzel, E. D. Electrochemical and Mechanical Behavior in Mechanically Robust Solid Polymer Electrolytes for Use in Multifunctional Structural Batteries. *Chem. Mater.* 2007, 19 (15), 3793–3801.
- (9) Xu, H. S; Yang, C. Z. The Ionic Conductive Property of Sulfonated Polyethylene Oxide Polyurethane Ionomers. *J. Polym. Sci. Part B Polym. Phys.* **1995**, *33* (5), 745–751.
- (10) Das, S.; Ghosh, A. Effect of Plasticizers on Ionic Conductivity and Dielectric Relaxation of PEO-LiClO₄ Polymer Electrolyte. *Electrochim. Acta* **2015**, *171*, 59–65.
- (11) Zhang, S.; Lee, K. H.; Frisbie, C. D.; Lodge, T. P. Ionic Conductivity, Capacitance, and Viscoelastic Poperties of Block Copolymer-Based Ion Gels. *Macromolecules* **2011**, *44*

- (4), 940-949.
- (12) Lodge, T. P.; Ueki, T. Mechanically Tunable, Readily Processable Ion Gels by Self-Assembly of Block Copolymers in Ionic Liquids. *Acc. Chem. Res.* **2016**, *49* (10), 2107–2114.
- (13) Susan, M. A. B. H.; Kaneko, T.; Noda, A.; Watanabe, M. Ion Gels Prepared by in Situ Radical Polymerization of Vinyl Monomers in an Ionic Liquid and Their Characterization as Polymer Electrolytes. *J. Am. Chem. Soc.* **2005**, *127* (13), 4976–4983.
- (14) Wang, Y.; Chen, Y.; Gao, J.; Yoon, H. G.; Jin, L.; Forsyth, M.; Dingemans, T. J.; Madsen, L. A. Highly Conductive and Thermally Stable Ion Gels with Tunable Anisotropy and Modulus. *Adv. Mater.* 2016, 28 (13), 2571–2578.
- (15) Watanabe, M.; Thomas, M. L.; Zhang, S.; Ueno, K.; Yasuda, T.; Dokko, K. Application of Ionic Liquids to Energy Storage and Conversion Materials and Devices. *Chem. Rev.* 2017, 117 (10), 7190–7239.
- (16) Eftekhari, A.; Liu, Y.; Chen, P. Different Roles of Ionic Liquids in Lithium Batteries. *J. Power Sources* **2016**, *334*, 221–239.
- (17) Lewandowski, A.; Świderska-Mocek, A. Ionic Liquids as Electrolytes for Li-Ion Batteries-An Overview of Electrochemical Studies. *J. Power Sources* 2009, 194 (2), 601–609.
- (18) Villanueva, M.; Coronas, A.; García, J.; Salgado, J. Thermal Stability of Ionic Liquids for Their Application as New Absorbents. *Ind. Eng. Chem. Res.* **2013**, *52* (45), 15718–15727.
- (19) Jeon, N.; Jo, S.; Kim, S.; Park, M.; Kim, D. Quasi-Solid-State Polymer Electrolytes Based on a Polymeric Ionic Liquid with High Ionic Conductivity and Enhanced Stability. *J. Electrochem. Sci. Technol* **2017**, *8* (3), 257–264.
- (20) He, Y.; Boswell, P. G.; Bühlmann, P.; Lodge, T. P. Ion Gels by Self-Assembly of a Triblock Copolymer in an Ionic Liquid. *J. Phys. Chem. B* **2007**, *111* (18), 4645–4652.
- (21) Zhang, R.; Chen, Y.; Montazami, R. Ionic Liquid-Doped Gel Polymer Electrolyte for

- Flexible Lithium-Ion Polymer Batteries. *Materials* **2015**, 8 (5), 2735–2748.
- (22) Wang, Y.; He, Y.; Yu, Z.; Gao, J.; Brinck, S. T.; Slebodnick, C.; Fahs, G. B.; Zanelotti, C. J.; Hegde, M.; Moore, R. B.; Ensing, B.; Dingemans, T. J.; Qiao, R; Madsen, L. A. Double Helical Conformation and Extreme Rigidity in a Rodlike Polyelectrolyte. *Nat. Commun.* 2019, *10*, 1–8. https://doi.org/10.1038/s41467-019-08756-3.
- (23) Yu, Z.; He, Y.; Wang, Y.; Madsen, L. A.; Qiao, R. Molecular Structure and Dynamics of Ionic Liquids in a Rigid-Rod Polyanion-Based Ion Gel. *Langmuir* **2017**, *33* (1), 322–331.
- (24) Berthier, C.; Gorecki, W.; Minier, M.; Armand, M. B.; Chabagno, J. M.; Rigaud, P. Microscopic Investigation of Ionic Conductivity in Alkali Metal Salts-Poly(Ethylene Oxide) Adducts. *Solid State Ionics* 1983, 11 (1), 91–95.
- (25) Armand, M. Polymers with Ionic Conductivity. *Adv. Mater.* **1990**, *2* (6–7), 278–286.
- (26) Wu, Z. L.; Arifuzzaman, M.; Kurokawa, T.; Le, K.; Hu, J.; Sun, T. L.; Furukawa, H.; Masunaga, H.; Gong, J. P. Supramolecular Assemblies of a Semirigid Polyanion in Aqueous Solutions. *Macromolecules* **2013**, *46* (9), 3581–3586.
- (27) Wang, Y.; Gao, J.; Dingemans, T. J.; Madsen, L. A. Molecular Alignment and Ion Transport in Rigid Rod Polyelectrolyte Solutions. *Macromolecules* 2014, 47 (9), 2984–2992.
- (28) Gao, J.; Wang, Y.; Norder, B.; Garcia, S. J.; Picken, S. J.; Madsen, L. A.; Dingemans, T. J. Water and Sodium Transport and Liquid Crystalline Alignment in a Sulfonated Aramid Membrane. *J. Memb. Sci.* 2015, 489, 194–203.
- (29) Fox, R. J.; Yu, D.; Hegde, M.; Kumbhar, A. S.; Madsen, L. A.; Dingemans, T. J. Nanofibrillar Ionic Polymer Composites Enable High Modulus Ion-Conducting Membranes. ACS Appl. Mater. Interfaces 2019, 11, 40551–40563.
- (30) Fam, W.; Mansouri, J.; Li, H.; Hou, J.; Chen, V. Gelled Graphene Oxide Ionic Liquid Composite Membranes with Enriched Ionic Liquid Surfaces for Improved CO 2 Separation. *Appl. Mater. Interfaces* **2018**, *10*, 7389–7400.

- (31) Ito, K.; Nishina, N.; Ohno, H. High Lithium Ionic Conductivity of Poly(Ethylene Oxide)s Having Sulfonate Groups on Their Chain Ends. *J. Mater. Chem.* **1997**, *7* (8), 1357–1362.
- (32) Magonov, S. N.; Elings, V.; Whangbo, M. Phase Imaging and Stiffness in Tapping-Mode Atomic Force Microscopy. *Surf. Sci.* **1997**, *375*, 385–391.
- (33) Devecchio, D.; Bhushan, B. Localized Surface Elasticity Measurements Using an Atomic Force Microscope. *Rev. Sci. Instrum.* **1997**, *68* (12), 4498–4505.
- (34) Williams, M. L.; Landel, R. F.; Ferry, J. D. The Temperature Dependence of Relaxation Mechanisms in Amorphous Polymers and Other Glass-Forming Liquids. *J. Am. Chem. Soc.* **1955**, *77* (12), 3701–3707.
- (35) Choi, U. H.; Ye, Y.; Salas De La Cruz, D.; Liu, W.; Winey, K. I.; Elabd, Y. A.; Runt, J.; Colby, R. H. Dielectric and Viscoelastic Responses of Imidazolium-Based Ionomers with Different Counterions and Side Chain Lengths. *Macromolecules* **2014**, *47* (2), 777–790.
- (36) Pogodina, N. V.; Nowak, M.; Läuger, J.; Klein, C. O.; Wilhelm, M.; Friedrich, C. Molecular Dynamics of Ionic Liquids as Probed by Rheology. *J. Rheol.* 2011, 55 (2), 241–256.
- (37) Weingärtner, H.; Sasisanker, P.; Daguenet, C.; Dyson, P. J.; Krossing, I.; Slattery, J. M.; Schubert, T. The Dielectric Response of Room-Temperature Ionic Liquids: Effect of Cation Variation. *J. Phys. Chem. B* **2007**, *111* (18), 4775–4780.
- (38) Hunger, J.; Stoppa, A.; Schrödle, S.; Hefter, G.; Buchner, R. Temperature Dependence of the Dielectric Properties and Dynamics of Ionic Liquids. *ChemPhysChem* **2009**, *10* (4), 723–733.
- (39) Rubinstein, M.; Colby, R. H. *Polymer Physics*; Oxford University Press: New York, 2003.
- (40) Mujtaba, A.; Keller, M.; Ilisch, S.; Radusch, H. J.; Thurn-Albrecht, T.; Saalwächter, K.; Beiner, M. Mechanical Properties and Cross-Link Density of Styrene-Butadiene Model Composites Containing Fillers with Bimodal Particle Size Distribution. *Macromolecules* 2012, 45 (16), 6504–6515.

- (41) Cervenka, A. PEEK/Carbon Fiber Composites: Experimental Evaluation of Unidirectional Laminates and Theoretical Prediction of Their Properties. *Polym. Compos.* **1988**, *9* (4), 263–270.
- (42) Kremer, F.; Schonhals, A. *Broadband Dielectric Spectroscopy*; Springer Verlag Berlin Heidelberg: New York, 2003.
- (43) Chen, Q.; Bao, N.; Wang, J. H. H.; Tunic, T.; Liang, S.; Colby, R. H. Linear Viscoelasticity and Dielectric Spectroscopy of Ionomer/Plasticizer Mixtures: A Transition from Ionomer to Polyelectrolyte. *Macromolecules* **2015**, *48* (22), 8240–8252.
- (44) Leys, J.; Wübbenhorst, M.; Preethy Menon, C.; Rajesh, R.; Thoen, J.; Glorieux, C.; Nockemann, P.; Thijs, B.; Binnemans, K.; Longuemart, S. Temperature Dependence of the Electrical Conductivity of Imidazolium Ionic Liquids. *J. Chem. Phys.* **2008**, *128* (6), 1–7.
- (45) Krause, C.; Sangoro, J. R.; Iacob, C.; Kremer, F. Charge Transport and Dipolar Relaxations in Imidazolium-Based Ionic Liquids. *J. Phys. Chem. B* **2010**, *114* (1), 382–386.
- (46) Sun, L.; Morales-Collazo, O.; Xia, H.; Brennecke, J. F. Effect of Structure on Transport Properties (Viscosity, Ionic Conductivity, and Self-Diffusion Coefficient) of Aprotic Heterocyclic Anion (AHA) Room-Temperature Ionic Liquids. 1. Variation of Anionic Species. J. Phys. Chem. B 2015, 119 (48), 15030–15039.
- (47) Choi, U. H.; Mittal, A.; Price, T. L.; Gibson, H. W.; Runt, J.; Colby, R. H. Polymerized Ionic Liquids with Enhanced Static Dielectric Constants. *Macromolecules* **2013**, *46* (3), 1175–1186.
- (48) Choi, U. H.; Colby, R. H. The Role of Solvating 12-Crown-4 Plasticizer on Dielectric Constant and Ion Conduction of Poly(Ethylene Oxide) Single-Ion Conductors. *Macromolecules* **2017**, *50* (14), 5582–5591.
- (49) Tudryn, G. J.; Liu, W.; Wang, S. W.; Colby, R. H. Counterion Dynamics in Polyester-

- Sulfonate Ionomers with Ionic Liquid Counterions. *Macromolecules* **2011**, *44* (9), 3572–3582.
- (50) Tudryn, G. J.; O'Reilly, M. V.; Dou, S.; King, D. R.; Winey, K. I.; Runt, J.; Colby, R. H. Molecular Mobility and Cation Conduction in Polyether-Ester-Sulfonate Copolymer Ionomers. *Macromolecules* 2012, 45 (9), 3962–3973.
- (51) Sangoro, J.; Iacob, C.; Serghei, A.; Naumov, S.; Galvosas, P.; Kärger, J.; Wespe, C.; Bordusa, F.; Stoppa, A.; Hunger, J.; et al. Electrical Conductivity and Translational Diffusion in the 1-Butyl-3-Methylimidazolium Tetrafluoroborate Ionic Liquid. *J. Chem. Phys.* **2008**, *128* (21).
- (52) Stoppa, A.; Hunger, J.; Buchner, R.; Hefter, G.; Thoman, A.; Helm, H. Interactions and Dynamics in Ionic Liquids. *J. Phys. Chem. B* **2008**, *112* (16), 4854–4858.
- (53) Wheatle, B. K.; Keith, J. R.; Mogurampelly, S.; Lynd, N. A.; Ganesan, V. Influence of Dielectric Constant on Ionic Transport in Polyether-Based Electrolytes. *ACS Macro Lett.* 2017, 6 (12), 1362–1367.
- (54) Hou, J.; Zhang, Z.; Madsen, L. A. Cation/Anion Associations in Ionic Liquids Modulated by Hydration and Ionic Medium. *J. Phys. Chem. B* **2011**, *115* (16), 4576–4582.
- (55) Zhang, Z.; Madsen, L. A. Observation of Separate Cation and Anion Electrophoretic Mobilities in Pure Ionic Liquids Observation of Separate Cation and Anion Electrophoretic Mobilities. *J. Chem. Phys.* 2014, 140, 084204.
- (56) Lafemina, N. H.; Chen, Q.; Colby, R. H.; Mueller, K. T. The Diffusion and Conduction of Lithium in Poly(Ethylene Oxide)-Based Sulfonate Ionomers. *J. Chem. Phys.* 2016, 145 (11), 114903.
- (57) Lafemina, N. H.; Chen, Q.; Mueller, K. T.; Colby, R. H. Diffusive Flux as a New Metric for Ion-Conducting Soft Materials. *ACS Energy Lett.* **2016**, *1* (6), 1179–1183.
- (58) Abbrent, S.; Greenbaum, S. Recent Progress in NMR Spectroscopy of Polymer Electrolytes for Lithium Batteries. *Curr. Opin. Colloid Interface Sci.* **2013**, *18* (3), 228–244.

- (59) Murch, G. E. The Haven Ratio in Fast Ionic Conductors. *Solid State Ionics* **1982**, *7* (3), 177–198.
- (60) Frömling, T.; Kunze, M.; Schönhoff, M.; Sundermeyer, J.; Roling, B. Enhanced Lithium Transference Numbers in Ionic Liquid Electrolytes. *J. Phys. Chem. B* **2008**, *112* (41), 12985–12990.
- (61) Tokuda, H.; Hayamizu, K.; Ishii, K.; Bin, M. A.; Susan, H.; Watanabe, M.
 Physicochemical Properties and Structures of Room Temperature Ionic Liquids . 1 .
 Variation of Anionic Species. J. Phys. Chem. B 2004, 108 (42), 16593–16600.
- (62) Reiche, A.; Cramer, T.; Fleischer, G.; Sandner, R.; Sandner, B.; Kremer, F.; Ka, J. Ionic Conductivity-Structure Property Relationship in Gel Electrolytes on the Basis of Oligo(Ethylene Glycol)₂₃ Dimethacrylate Plasticized with Oligo(Ethylene Glycol)₁₁ Dimethyl Ether. *J. Phys. Chem.* **1997**, *4* (97), 1861–1869.

ToC Graphic: for Table of Contents only

